COLLECTIVE BEHAVIOR

Reverse engineering the control law for schooling in zebrafish using virtual reality

Liang Li[1,2,3,4]*, Máté Nagy[1,2,3,5,6]*, Guy Amichay[1,2,3,7,8,9], Ruiheng Wu[1,2,4], Wei Wang[10], Oliver Deussen[2,4], Daniela Rus[11], Iain D. Couzin[1,2,3]*

Revealing the evolved mechanisms that give rise to collective behavior is a central objective in the study of cellular and organismal systems. In addition, understanding the algorithmic basis of social interactions in a causal and quantitative way offers an important foundation for subsequently quantifying social deficits. Here, with virtual reality technology, we used virtual robot fish to reverse engineer the sensory-motor control of social response during schooling in a vertebrate model: juvenile zebrafish (*Danio rerio*). In addition to providing a highly controlled means to understand how zebrafish translate visual input into movement decisions, networking our systems allowed real fish to swim and interact together in the same virtual world. Thus, we were able to directly test models of social interactions in situ. A key feature of social response is shown to be single- and multitarget-oriented pursuit. This is based on an egocentric representation of the positional information of conspecifics and is highly robust to incomplete sensory input. We demonstrated, including with a Turing test and a scalability test for pursuit behavior, that all key features of this behavior are accounted for by individuals following a simple experimentally derived proportional derivative control law, which we termed "BioPD." Because target pursuit is key to effective control of autonomous vehicles, we evaluated—as a proof of principle—the potential use of this simple evolved control law for human-engineered systems. In doing so, we found close-to-optimal pursuit performance in autonomous vehicle (terrestrial, airborne, and watercraft) pursuit while requiring limited system-specific tuning or optimization.

INTRODUCTION

Collective behavior arises from positive and/or negative local feedback loops, which enable repeated local interactions to scale up into highly robust coordinated activities without the need for regulation by global supervision or via a preestablished template (*1*, *2*). Given their ubiquity and importance across scales of biological organization, the mechanisms that give rise to coordinated motion among cells (*3*) and organisms such as swarming insects (*4*, *5*), schooling fish (*6*–*8*), flocking birds (*9*, *10*), and humans in crowds (*11*, *12*) have been of particular interest across multiple disciplines. In addition to providing deeper insights into biology, an understanding of the evolved strategies animals use to coordinate collective behavior can offer new opportunities for the development of engineered solutions (*13*), such as for the coordination of autonomous vehicles (*14*, *15*).

To date, however, it has been extremely difficult to infer the nature and causal structure of biological interactions that give rise to collective behavior using conventional experimental approaches (*16*–*18*). Consequently, the sensory-motor feedback mechanisms that have evolved to regulate collective behavior are often poorly understood (*19*), with our inability to identify, or test among, alternative hypotheses being a major bottleneck. Recent advances in immersive volumetric virtual reality (VR) technology (*20*–*22*) provide a new means to control, and thus interrogate, the causal structure of social relationships among individuals. In addition, they allow the direct testing of experimentally derived hypothetical models of social interactions in situ by allowing reciprocal coupling between real organisms and virtual robot fish as counterparts (*23*). Thus, analogous to how the dynamic patch clamp method has revolutionized neuroscience, creating a real-time interface between living cells and experimentally derived models (*24*), VR opens up a dynamic social clamp approach (*23*) to the study of animal behavior.

In this study, we applied a VR platform (*20*) to control virtual conspecifics that can interact with real fish (RF), enabling us to reverse engineer the fundamental sensory-motor control (SMC) mechanisms governing leader-follower dynamics under various conditions (Fig. 1A, fig. S1, and Movie 1). We found that a simple, yet powerful, proportional derivative–like controller, which we term "BioPD," effectively captures the social pursuit behavior of fish (Fig. 1, B to D). To validate the model, we explored its assumptions, assessed its predictive capabilities, and conducted a Turing test with RF—all of which confirmed the model's effectiveness (Fig. 1, D to F). Last, we applied BioPD to different robotic systems, tested the scalability of the model in large-scale fish schools across different species, and integrated it into various robotic platforms for diverse group sizes and pursuit tasks (Fig. 1, G to I). Our findings highlight the potential of robotic platforms, such as VR, as valuable tools for understanding collective behavior while, simultaneously, in return, inspiring advancements in robotic control design.

[1]Department of Collective Behaviour, Max Planck Institute of Animal Behavior, 78464 Konstanz, Germany. [2]Centre for the Advanced Study of Collective Behaviour, University of Konstanz, 78464 Konstanz, Germany. [3]Department of Biology, University of Konstanz, 78464 Konstanz, Germany. [4]Department of Computer and Information Science, University of Konstanz, 78464, Konstanz, Germany. [5]MTA-ELTE "Lendület" Collective Behaviour Research Group, Hungarian Academy of Sciences, 1117 Budapest, Hungary. [6]Department of Biological Physics, Eötvös Loránd University, 1117 Budapest, Hungary. [7]Department of Engineering Sciences and Applied Mathematics, Northwestern University, Evanston, IL 60208, USA. [8]Northwestern Institute on Complex Systems, Northwestern University, Evanston, IL 60208, USA. [9]National Institute for Theory and Mathematics in Biology, Northwestern University, Evanston, IL 60208, USA. [10]Department of Mechanical Engineering, University of Wisconsin–Madison, Madison, WI 53706, USA. [11]Computer Science and Artificial Intelligence Lab (CSAIL), Massachusetts Institute of Technology, Cambridge, MA 02139, USA.
*Corresponding author. Email: lli@ab.mpg.de (L.L.); mate.nagy@ttk.elte.hu (M.N.); icouzin@ab.mpg.de (I.D.C.)

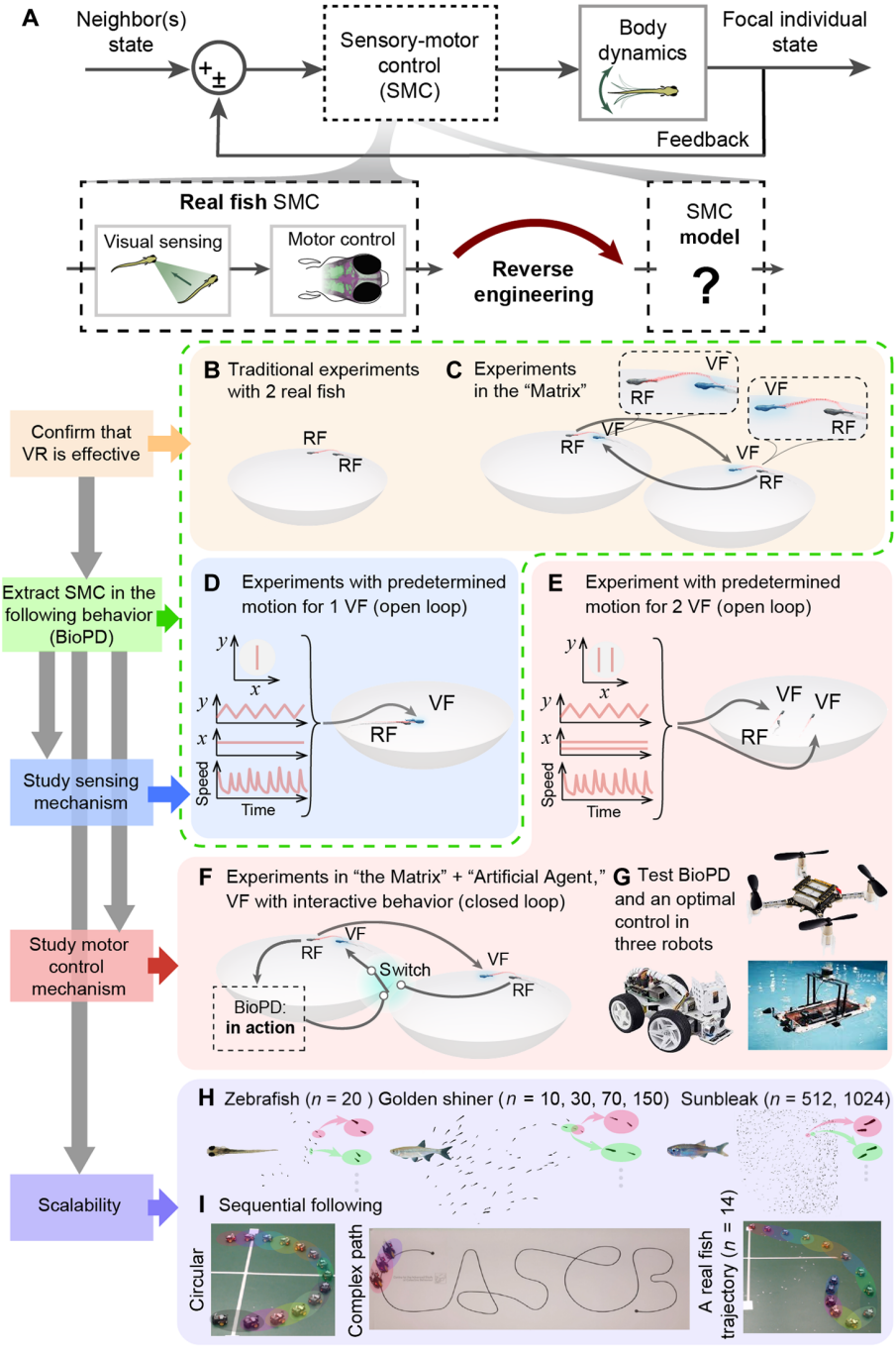

Fig. 1. Schematic of the study of SMC of schooling behavior. (**A**) The flow diagram of the SMC of the social response to neighbors. We reverse engineered the sensory-motor control (SMC) of following behavior to a model, which we term BioPD. (**B**) Traditional experiment in which two RF swim together in one bowl-shaped arena. Note that the lines trailing each fish indicate their movement trajectories, which are shown at a 1:1 scale relative to the dimensions of the bowl. The fish themselves are enlarged by a factor of 3 to ensure better visibility. (**C**) The Matrix system, where each arena contains a single individual, each of which can interact with a real-time volumetric projection of the other. (**D**) Open-loop experiments with one VF as a leader swimming back and forth at a recorded swimming speed (0.04 m/s in average). (**E**) Experiments with two VF swimming side by side as two leaders to verify the SMC. (**F**) Experiments with two RF interacting within the Matrix to verify the SMC of the following behavior. A VF becomes a follower controlled by the BioPD when the RF becomes a leader (when the RF swims in front). Otherwise, the VF copies the position and direction of the RF in the other arena. (**G**) Evaluating the performance of the BioPD model by comparing it with an MPC in three robotic systems (terrestrial, airborne, and watercraft). (**H** and **I**) Evaluating BioPD's scalability across three species in groups up to 1024 individuals and with up to 14 robots.

RESULTS

Development and validation of the immersive VR system

We applied an immersive VR for fish (*20*) to investigate the SMC used in regulating schooling behavior in a model vertebrate, the juvenile zebrafish (*Danio rerio*) (1 ± 0.1 cm in length, 24 to 26 days postfertilization; Fig. 1 and Movie 2). At this age, zebrafish predominantly use vision to coordinate response to conspecifics when schooling [the lateral line being dominated by self-generated motion because of viscous adhesion forming a boundary layer around such small fish (*25*)].

Given that leading others is known to be driven by different internal processes, such as indifference to others (*26*) and motion toward external goals (*27*), as a valuable starting point—and because of their general importance—we focus here only on socially mediated interactions. In addition to uncovering a key algorithm used in regulating schooling behavior (Fig. 1, B to F and H, Supplementary Methods, fig. S1, and table S1), we demonstrated its application to motion control in engineered systems (Fig. 1, G and I).

Because our immersive VR, for freely swimming animals, relies on correct volumetric rendering from the perspective of a single individual (via the anamorphic illusion), it is not possible to put more than one individual in each VR arena. We can, however, connect systems (*28*) such that individuals can see, and thus interact with, a real-time "holographic" projection of the other (Fig. 1C shows this principle for a pair of individuals), which we term "the Matrix" (Movie 2). We found that as in the real world (figs. S2, A to D; S3, A to D; and S4, A and C), individuals in "the Matrix" (figs. S2, E to H; S3, E to H; and S4, B and D) interact only when they occupy the same x-y plane, with even small movements out of that plane (in the z dimension), either toward the surface or to deeper water, being associated with rapid decoupling of social interactions (fig. S5). The structure, and strength, of the interactions within this plane [as quantified by decomposing motion to lateral speed v_x, which is perpendicular to the leader's head direction, and forward speed v_y, which is along the leader's head direction (Fig. 2A)] is found to be near identical when they interact within the physical world (fig. S4, A and C) as when they interact in the same holographic world (figs. S4, B and D, and S6; Kolmogorov-Smirnov test, $P = 0.26$ for v_x and $P = 0.9$ for v_y). This suggests that our VR system is ideal for dissecting sensory-motor feedback control.

Reverse engineering the control law for schooling in zebrafish using virtual reality

L. Li, M. Nagy, G. Amichay, R. Wu, W. Wang,
O. Deussen, D. Rus & I. D. Couzin

2025

Science Robotics
AAAS

Centre for the Advanced Study of Collective Behaviour
Universität Konstanz
MAX PLANCK INSTITUTE OF ANIMAL BEHAVIOR
HUNGARIAN ACADEMY OF SCIENCES
Eötvös Loránd University
WISCONSIN
Massachusetts Institute of Technology

Movie 1. Summary video. Video abstract of the study.

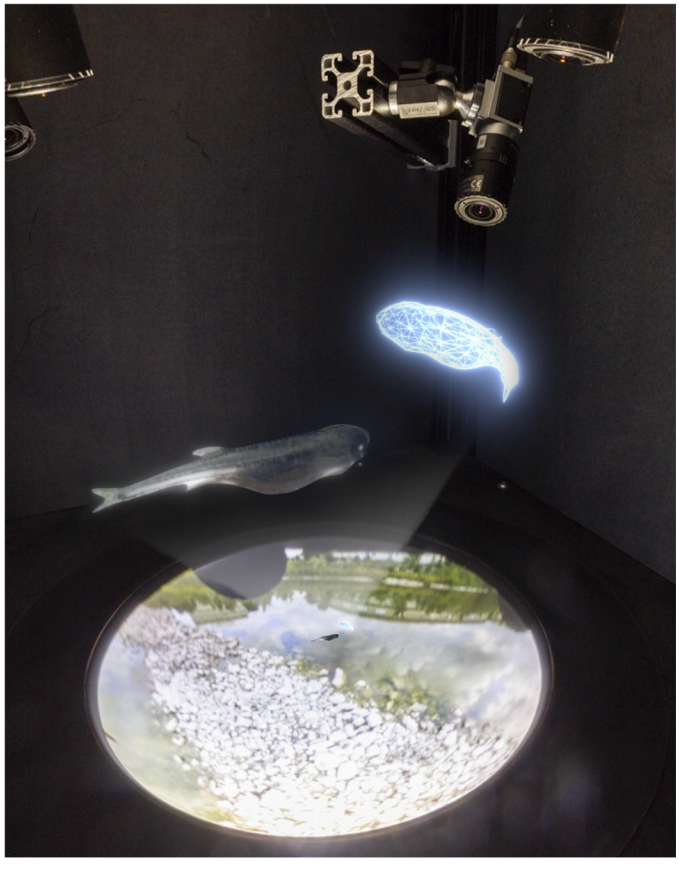

Movie 2. Overview of the experiments with VF interacting with RF. Variety of experiments using our VR platform for freely swimming zebrafish, including platform validation in the Matrix; one VF with varying average speeds, movement patterns, update rates, and visibilities; a Turing test in the Matrix; and two VF with different average speeds.

Reverse engineering the sensory-motor feedback control

To do so, we first conducted open-loop experiments, which allow us to control the causal flow of information from a leading (virtual) fish to a following (real) fish (Fig. 2B). Our platform also enables us to isolate and analyze how social responses are influenced by both spatial factors and average swim speed. Here, we evaluated average swim speed across its natural range while also accounting for its inherently bursty nature—characterized by rapid tail undulations followed by a friction-dominated glide (Fig. 2C and fig. S7).

Fish tend to follow/pursue the virtual leader at a relatively stable distance, with this distance increasing approximately linearly as a function of the leader's speed (Fig. 2, D to J, and fig. S8), but with different "times to collision" (with respect to the current position of the leader, if the leader were to suddenly stop; fig. S9). The decomposed lateral (v_x) and forward (v_y) components of the follower's speed, as a function of the spatial position of the follower relative to a leader positioned at $x = 0$ and $y = 0$, are shown in Fig. 2 (E and F, respectively). As shown in Fig. 2G, the average lateral speed increases as a function of lateral distance (x axis) up to a specific distance, $r_x = 0.07$ m (determined by finding the maximum lateral speeds following a bootstrapping procedure; see Supplementary Methods for details), indicated by the dotted line, after which it starts to decrease. Lateral speed is minimally influenced by swim speed (as seen by the similarity of panels in Fig. 2E and the average plots in Fig. 2G). The magnitude of the forward speed component as a function of the front-back distance, shown in Fig. 2H, also increases up to a similar distance, $r_y = 0.07$ m (see Supplementary Methods for details), but unlike lateral speed, it increases in absolute magnitude as a function of average swim speed of the leader.

According to the above properties (speed control being proportional to the distance lag and to the average swimming speed of the leader and a lateral point of speed reduction at a specific distance) and following reverse engineering methods in biological studies (*29*–*35*), we proposed a parsimonious bioinspired proportional-derivative (PD) controller, BioPD

$$\begin{cases} x_e = x_\mathrm{F} - x_\mathrm{L} \\ v_x = -\left(K_\mathrm{p} x_e + K_\mathrm{d} \dot{x}_e\right) e^{-\frac{x_e^2}{2r_x^2}} \\ y_e = y_\mathrm{F} - y_\mathrm{L} \\ v_y = -\left(K_\mathrm{p} y_e + K_\mathrm{d} \dot{y}_e\right) e^{-\frac{y_e^2}{2r_y^2}} \end{cases} \quad (1)$$

where x_F and y_F (and, respectively, x_L and y_L) are the positions of the follower (leader) in a global coordinate system resolved in the x and y axes according to the leader, respectively (Fig. 2A). r_x and r_y describe the critical distances at which the strength of social interactions is the largest (Supplementary Methods). K_d and K_p are the derivative gain and proportional gain parameters, respectively, which are the two main parameters in the model. We first determined the derivative parameter on the basis of the relationship between the average

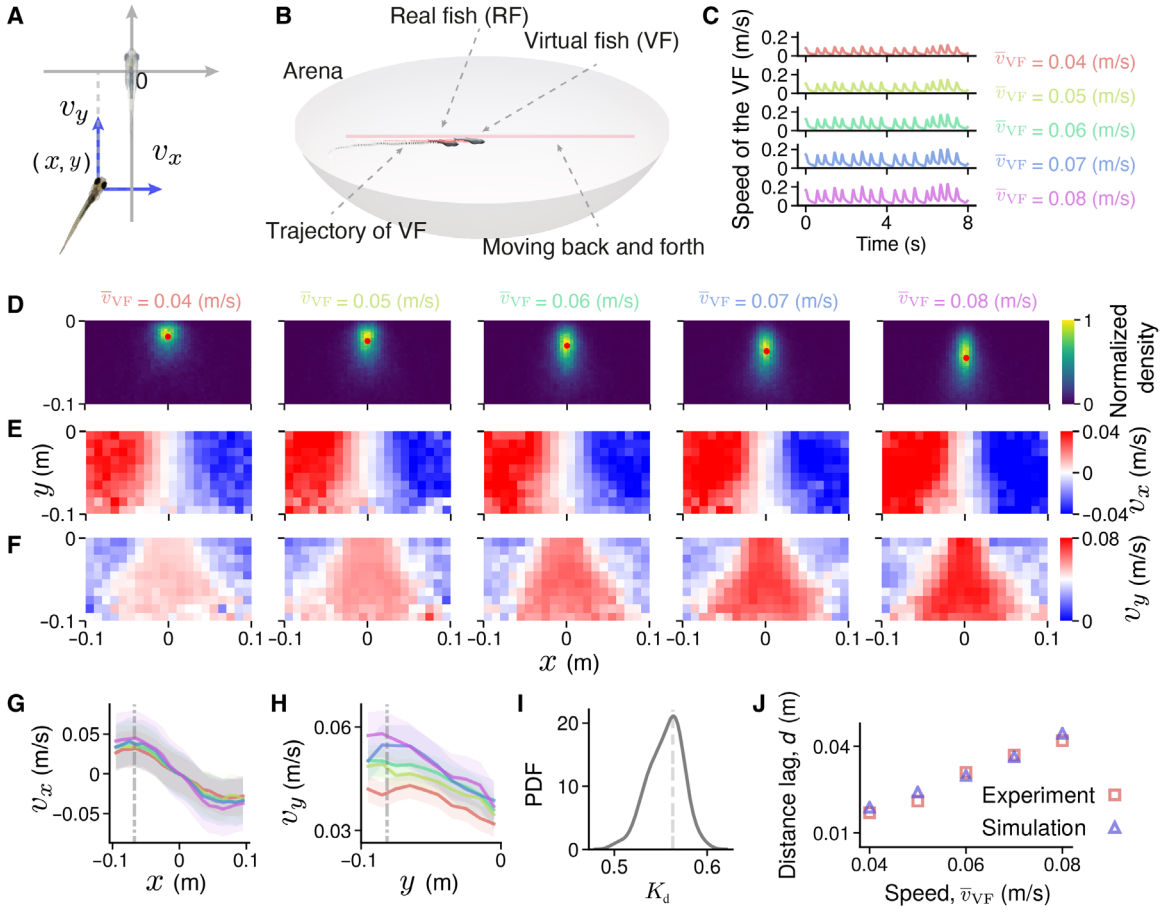

Fig. 2. Reverse engineering SMC of fish to a bioinspired proportional-derivative controller, BioPD. (**A**) The local coordinate system is based on the position and direction of the leader. The RF's swimming speed is resolved into lateral speed v_x and forward speed v_y. (**B**) Schematic to show the experimental setup, where an RF follows one VF that is swimming back and forth in a straight line. (**C**) The VF exhibits a realistic burst-and-glide swimming pattern for five different average swimming speeds $\overline{v}_{VF}$ (0.04 to 0.08 m/s with an interval of 0.01 m/s). (**D**) The higher the average swimming speed of the leader, the greater the distance maintained by the follower to the leader. (**E** and **F**) Lateral (E) and forward (F) speed control as a function of the position of the follower in the local coordinate of the leader with different average swimming speeds. (**G** and **H**) Average lateral (G) and forward (H) speeds as a function of the follower's position in the x (G) and y (H) axes in the local coordinate of the leader. The shaded areas denote the standard deviation after 100 bootstraps. In general, the lateral swimming speed, v_x, is less sensitive to the leader's average swimming speed, because there is no difference in both the density (E) and average plots (G). However, the forward speed, v_y, shows sensitivity in both the density (F) and average plots (H). (**I**) The distribution of the derivative parameter K_d is based on the maximum forward swimming speed at each average swimming speed of the leader. PDF, probability density function. (**J**) The comparison between the experiments and simulations shows that the model describes the experimental data.

forward swimming speed of RF and virtual fish (VF) (see Supplementary Methods for details), finding $K_d = 0.56$ (Fig. 2I). The proportional parameter K_p was estimated on the basis of the stable distance lag under different average swimming speeds of the leader, which for our zebrafish was found to be a constant with value $K_p = 2.3$ (Fig. 2J).

Despite its simplicity, we found that the BioPD model can account for all of the main features observed in our experiments, including the stable swim speed of the follower, which is matched to that of the leader (fig. S10, A and B), a similar spatial probability density with respect to the leader, and similar lateral and forward swimming speeds as a function of x_e and y_e (fig. S10, C to F). This indicates that a simple PD-like controller, with identical parameters, can effectively regulate schooling fish, irrespective of the average swim speed of the leader.

Validation of the assumptions of the BioPD model

Speed input in a PD controller can be either the instantaneous speed or the average speed over some period of time, as perceived directly through the fish's vision. Therefore, we further used our virtual robotic conspecifics to evaluate, directly, which features of the speed of conspecifics are used in regulating social response. Previously, it has been suggested that the motion characteristics associated with burst-and-glide locomotion of juvenile zebrafish may provide an important social cue (*36*). However, using VF swimming with burst and glide as the control [Fig. 3A(i)] and constant-speed swimming at the same average speed as the treatment [Fig. 3A(ii) and Movie 2], we observed that the following distance lag [Fig. 3A(iii) versus (iv)], lateral speed [Fig. 3A(v) versus (vi)], and forward speed [Fig. 3A(vii) versus (viii)] are the same. This indicates that zebrafish respond similarly to continuous motion as they do to biological (bursty) motion (see fig. S11 for a detailed comparison).

This suggests that fine-scale instantaneous speed is not used in the regulation of schooling. To evaluate this further, we investigated how the temporal resolution of visual input influences social response. By systematically changing the temporal update frequency,

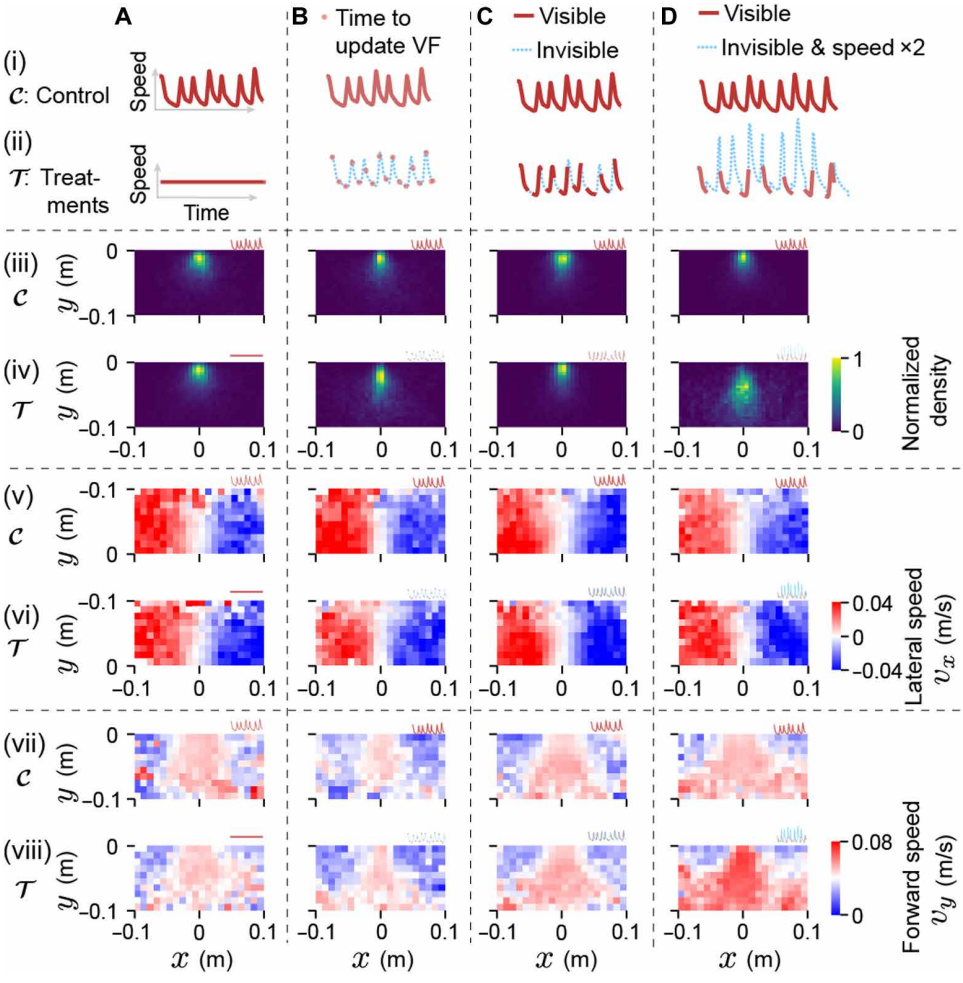

Fig. 3. Evaluating the perceptual information used in the regulation of social response to a leader. (**A**) VF swims with the same average but different instantaneous speeds: burst and glide as the control (i) or constant speed as the treatment (ii). (**B**) VF swims with different update frequencies at 100 Hz as the control (i) or at 5 Hz as the selected treatment (ii) while keeping a fixed location between updates. (**C**) VF swims with different visibilities [always visible as the control (i) or periodically become invisible (times being visible and invisible are both set to 0.2 s) as the treatment (ii)] to decouple the presented position and speed information. (**D**) Same as (C), except the VF jumps to a location further away by increasing its speed during the period of invisibility by a factor of 2 as compared with speed during being visible. Selected swimming performances, including relative position (iii and iv), lateral speed (v and vi), and forward speed (vii and viii), are presented.

such that the VF is always visible but its position is only updated at a certain rate (for instance, if the frequency is 10 Hz, the position of the VF will be updated 10 times per second, the frames between which it does not change position; fig. S12 and Movie 2), we found that only if the update rate falls below ~5 Hz does the distance lag increase [Fig. 3B(iii) to (iv)], indicating a diminishing of the effectiveness of the social response below this frequency (Fig. 3B). This indicates that zebrafish integrate information over ~0.2 s, a timescale close to the typical period of their burst-and-glide gait (fig. S7), which may imply the use of spatial working memory (*37*) and is captured in the model by averaging speed with a similar time window.

To establish how robust the schooling response is in the face of incomplete information, we decoupled speed and position by manipulating the visibility of the VF. As may be expected of animals that need to deal with regular occlusions of others, such as by vegetation or in patches of high turbidity, they do not respond to the sudden disappearance or appearance of a conspecific (Fig. 3, C and D, figs. S13 and S14, and Movie 2). By adjusting both the duration of the windows of time during which information is available (figs. S12 and S13) and whether the perceived speed in these windows is [Fig. 3C(ii)] or is not [Fig. 3D(ii)] congruent with the displacement (such as the average speed) between these windows (fig. S14), we observed no difference in distance lag, lateral speed, or forward speed when the perceived speed matches the invisible case [Fig. 3C(iii) to (viii)]. However, there was a substantial difference in the nonmatching case [Fig. 3D(iii) to (viii)]. This suggests that the algorithm used by zebrafish uses positional information as the input for speed control and not estimates of instantaneous speed (Fig. 3, C and D, and figs. S13 and S14).

Predictive power of BioPD

With the core assumptions of BioPD validated, we then asked whether it can account for further dynamical features of natural schooling. To establish the above control law, we used virtual robot fish as conspecifics that move in a constant direction and at a constant average swim speed. In reality, however, fish dynamically modulate both properties. By presenting exactly the same trajectories, obtained from RF leaders, both to RF and to agents using BioPD (Fig. 4, A and B), we compared directly the response of real followers with agents using BioPD. We found that BioPD provides a robust and effective response to the dynamic changes in speed and direction exhibited in the natural system and results in pursuit behavior highly comparable to that exhibited by RF (Fig. 4, E and F).

Our VR systems allow us to take an even further step in establishing SMC; we could also ask whether leaders react differently to real followers versus followers using BioPD. This can be thought of as a Turing test for the leader: Is an agent using BioPD sufficiently convincing to allow natural bidirectional interactions? To do so, we then allow two RF, A and B, to interact in the Matrix, but each time fish A becomes a leader (such as when it occupies a frontal position), we can immediately replace the natural control of B with our BioPD control (Fig. 4, C and D, fig. S15, and Movie 2). Thus, we compared what we predicted fish would do with what they actually did for every pursuit event. We found that despite its simplicity, BioPD facilitates the maintenance of qualitatively similar, and effective, reciprocal social relationships among hybrid simulated-real individuals (Fig. 4, G and H).

Having established the response to a single conspecific, we then asked whether BioPD can also predict the response of RF to two virtual conspecifics (*38*). To do so, we considered its response to two

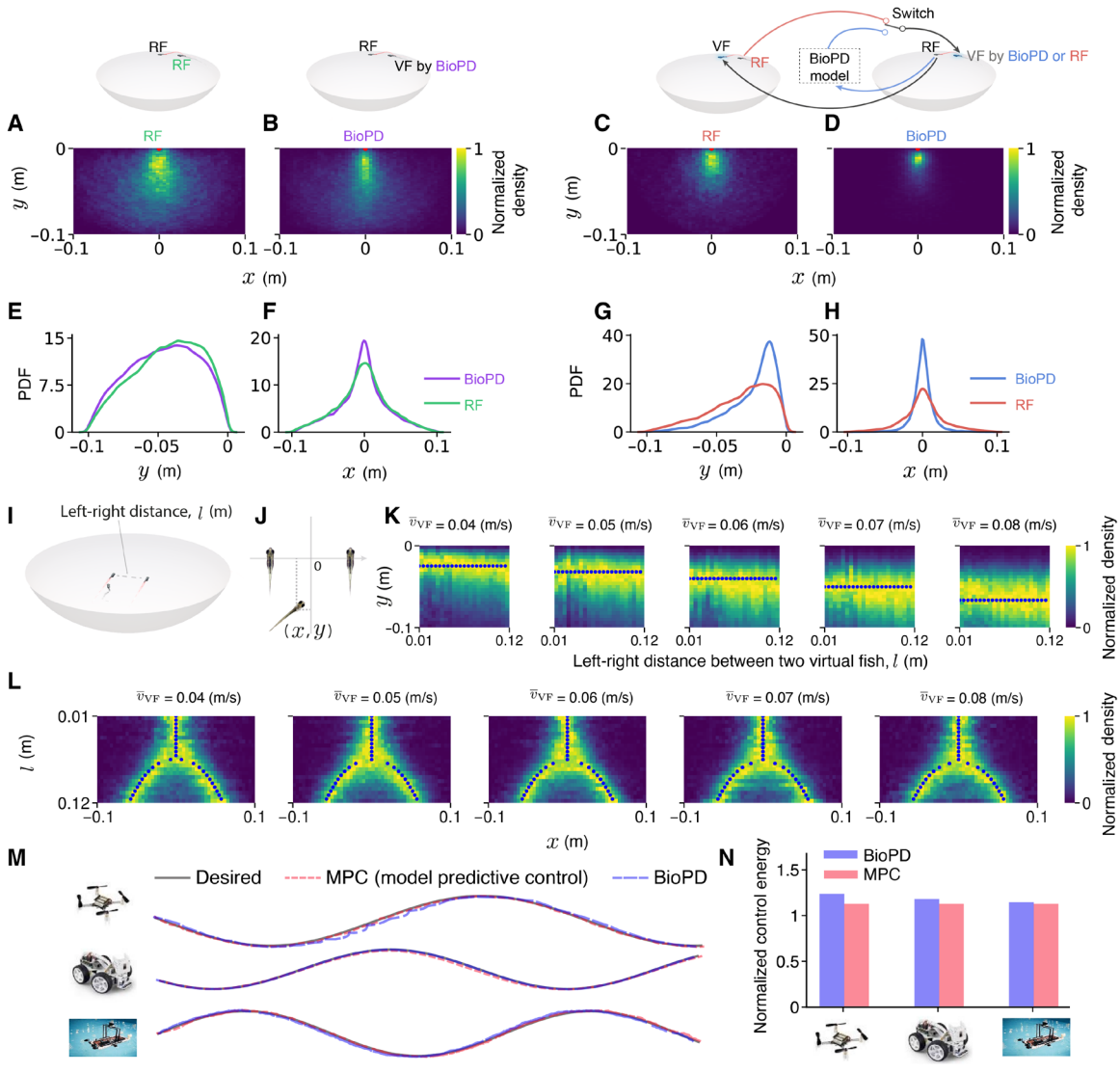

Fig. 4. Evaluating the BioPD: simulations, experiments in the Matrix system and in two virtual leader scenarios, and using robotics. (**A** and **B**) Positions of RF (A) as followers and simulated followers controlled by the BioPD [VF (B)] relative to a real leading fish (positioned at the origin). (**C** and **D**) Real (C)/virtual (D) follower's positions relative to the virtual (C)/real (D) leader's position in two arenas in the Matrix system. The VF in (D) represents an avatar of the RF from (C), unless the RF in (D) is swimming in front. In that case, the VF in (D) is controlled by BioPD. The VF in (C) is always controlled by the RF from (D). The RF in (C) follows the VF (C), which represents the RF shown in (D). (**E** to **H**) Distributions of relative distance in the *y* [(E) and (G)] and *x* [(F) and (H)] axes of the simulations [(E) and (F)] and experiments [(G) and (H)]. JSD = 0.03, 0.0, 0.08, and 0.0 for (E) to (H), respectively. (**I**) Setup for two VF leaders swimming side by side at different left-right distances and average swimming speeds. (**J**) Definition of the coordinate system. The origin is the center of the two VF. Positive *y* points to the head direction of the VF. (**K**) The model predicts the relative distance between the RF and the VF swimming at different average swimming speeds. (**L**) The model also predicts the bifurcations in the following behavior of the RF when they follow two virtual leaders. (**M**) Three robots are controlled by BioPD and MPC to follow a virtual leader moving in a sinusoidal wave. (**N**) Comparison of the control energy of BioPD and MPC.

leaders swimming side by side at a range of interindividual lateral distances and swim speeds (Fig. 4, I and J, and Movie 2). We simply applied the BioPD controller for an agent receiving sensory input from the two leaders but taking into account the linear perspective in the fish eye (see Supplementary Methods for details). We found that BioPD accounts, quantitatively, for a key experimental finding, given that the blue points predicted by the model match the high-density regions of RF behavior data in Fig. 4 (K and L); that RF will both change their distance lag (Fig. 4K) and suddenly switch from adopting a position in between the targets (here, the leaders) to deciding among them (swimming predominantly with one of the VF) as a function of increasing the lateral distance (l) between the virtual leaders (Fig. 4L and fig. S16). Furthermore, it also accounts for the observed increase in the critical distance (l_c) at which this transition occurs as a function of increasing swim speed (Fig. 4L and figs. S17 to S19).

Scalability of BioPD

To investigate the scalability and generalizability of our BioPD and its potential in elucidating collective behavior in large groups, we analyzed the social response of followers in schools of juvenile

zebrafish (*D. rerio*, $n = 20$) tracked with custom code (*39*), juvenile golden shiners [*Notemigonus crysoleucas*; $n = 10$, 30, 70, and 150; data from previous publication (*40*)], and juvenile sunbleak (*Leucaspius delineatus*, $n = 512$ and 1024) tracked with custom code (*39*). Across all three species, we observed pervasive leader-following behavior, even in larger group sizes. Analogous to the two-fish system, the distance lag correlates with the leading fish's average swimming velocity. The follower's turning and forward speeds align with characteristics previously observed in our VR system (Fig. 5, A to C, and fig. S20). Such findings suggest that the BioPD derived from smaller groups can be extrapolated to larger collectives.

Robotic applications of BioPD

Reverse engineering natural control laws—which have been subject to evolution by natural selection for millennia—could, in principle, provide simpler and/or more robust solutions for human-engineered problems (*13*). The effective pursuit of mobile targets, along with the maintenance of appropriate spacing with respect to a target (which can include interception or pursuit while also avoiding collisions, for example), is a central challenge in the effective control of autonomous vehicles, such as self-driving cars and guided aircraft and spacecraft. Human-made controllers, such as the widely used model predictive controller (MPC) (*41*), have been shown to be optimal for certain tasks but typically are computationally expensive because MPCs are solving an optimization problem over a predicted horizon (predicting future system behavior over a defined time frame) at each control step. Moreover, MPCs need to be individually optimized—a very time-consuming process—for each specific application (because they depend on an accurate underlying model of the dynamical systems in which they are to be embedded). Natural systems, by contrast, are under selection to evolve highly robust and cheap strategies that approximate optimal solutions under a wide range of conditions. Seldom, however, are such evolved solutions evaluated in situ in real physical systems.

To gain insight into such potential application domains, we implemented and compared the pursuit performance of a state-of-the-art optimal MPC controller (see Supplementary Methods for details) and BioPD in three very different robotic platforms: terrestrial vehicles, airborne drones (*42*), and watercraft (Fig. 1H); the task was to follow a virtual leader on a predefined sine-shaped trajectory (Fig. 4M and Movie 3). Furthermore, unlike the MPC controller, which required a complex and time-consuming optimization procedure for each robotic system, we used BioPD with exactly the same parameters as estimated from zebrafish in all scenarios. We found that with suboptimal control parameters extracted from the biological system (figs. S21 and S22), and despite its simplicity, BioPD exhibits highly robust and effective performance, providing very close to optimal control energy (*43*) in the vehicle, drone, and roboboat control tasks (Fig. 4N and figs. S23 to S25). To further assess the scalability of BioPD (Movie 3), we used the BioPD to direct 14 robots in a sequential circular motion (Fig. 5D), three robots in tracing an intricate path of the letters associated with our research center, "CASCB" (Fig. 5E), and 14 robots in emulating RF trajectories (18× larger scale) at both constant (Fig. 5F) and varying speeds (Fig. 5G). The corresponding deviation of each robot's trajectory to the desired path, distance lag between successive pairs of robots in the sequence, moving speeds, and control energy are illustrated in Fig. 5 (H to K) and figs. S26 to S29.

DISCUSSION

In this study, we constructed a virtual robotic "conspecific" for juvenile zebrafish and used it to reverse engineer the algorithm used to regulate social response. After confirming that RF accept the virtual robotic fish as a conspecific at the behavioral level, we demonstrated

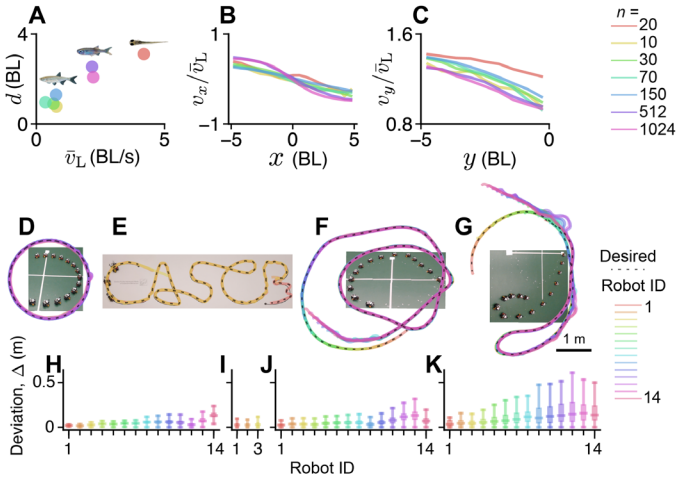

Fig. 5. Assessing the scalability of BioPD across three fish species (up to 1024 individuals) and robots (up to 14). (**A**) Distance lag plotted against the leader's average swimming speed. (**B** and **C**) Normalized turning speed, $u_x / \bar{u}_L$, and forward speed, $u_y / \bar{u}_L$, mapped to the left-right distance, x [body length (BL)], and front-back distance, y (BL), respectively. Data span three species: zebrafish (*D. rerio*, $n = 20$), golden shiner (*N. crysoleucas*, $n = 10$, 30, 70, and 150), and sunbleak (*L. delineatus*, $n = 512$ and 1024). (**D**) Group of robots exhibiting sequential circular motion. (**E**) Three robots tracing the intricate "CASCB" logo in sequence. (**F**) Fourteen robots sequentially emulating a constant-speed fish trajectory. (**G**) Fourteen robots mimicking a burst-and-coast fish trajectory, similar to natural fish movement patterns. Scale bar, 1 m [applies to (D) to (G)]. (**H** to **K**) Box plots featuring the median, interquartile range, and potential outliers are applied to illustrate the deviations (Δ) of each robot's trajectory from the desired path for conditions (D) to (G).

Movie 3. Overview of the experiments with robots controlled by BioPD for different pursuit behaviors. Series of experiments demonstrating the application of BioPD to robotic pursuit behaviors, including drone, terrestrial, and watercraft pursuits of a leader moving along a sinusoidal path; 14 robots engaged in sequential circular pursuit; three robots sequentially navigating complex letter-shaped trajectories; and 14 robots simulating RF movements at both constant and varying speeds.

that a simple PD-like controller (BioPD) can account for the social response exhibited toward it by RF (Fig. 2). Taking advantage of the virtual robot platform, we systematically checked the assumptions of the model (Fig. 3), verified the effectiveness of the model (Fig. 4, A to H), tested its power of prediction (Fig. 4, I to L), explored its potential applications (Fig. 4, M and N), and demonstrated its scalability (Fig. 5). These tests illustrate that the platform is a powerful tool for quantitatively and causally exploring hidden internal controls, offering capabilities that have been largely inaccessible in previous systems.

By controlling the visibility of the virtual robot to decouple position and speed perception [something not possible in traditional biological experiments or even with those physical replicas (*28*)], we found that fish primarily rely on position perception rather than instantaneous speed perception (Fig. 3). In addition, the input for derivative control on long-term average speed is derived from positional information (fig. S13). This mechanism is similar to a low-pass filter and could facilitate noise reduction in the velocity control. However, it remains unclear how fish obtain the neighbor's positional information from their visual scene, and this will be the focus of our future studies. Despite being derived from the response to a single leader, we found that BioPD can also account for the fish behavior when presented with two leaders: notably an abrupt transition (bifurcation) from averaging to deciding to follow one or the other of the potential leaders as a function of the distance between them (Fig. 4, I to L). This finding is consistent with our previous work on geometric principles that emerge from individual decision-making (*38*), where the linear distortion of perspective provides a comparable "non-Euclidean" distortion of space (*38*, *44*).

Our study suggests that fish may have evolved a sensorimotor control like BioPD given that it provides a cognitively minimal yet highly effective means to regulate schooling. Compared with traditional PD-like controllers in engineering systems (*45*, *46*), our controller differs in two key ways: First, it introduces a biologically meaningful cutoff in the interaction, embedded through a nonlinear first-order Gaussian function (Fig. 2, G and H), and second, it has been validated in biological systems through assumption verification (Fig. 3, A to D), predictive power testing (Fig. 4, I to L), and even an embodied Turing test (Fig. 4, A to H). This uniquely bridges engineering and biological systems. Unlike traditional PD controllers in biological systems that either explore PD functions within the system (*33*, *47*) or aim to find the best controllers to fit biological data (*30*, *48*, *49*), our approach focuses on reverse engineering the complete dynamics of pursuit behavior. We offer a detailed controller along with measured parameters, rather than merely fitting the data.

The reason BioPD generalizes well to the three robotic platforms may be the same reason it has evolved: Because the control is based on a kinematic model, without involving specific dynamics, it is highly generalized. Therefore, there is room for optimization for each robot based on the dynamic models of their respective systems (Fig. 4N and figs. S21 and S22), which will be our future focus. In the future, we will also explore in further detail the limitations and potential applications of this controller. In our preliminary analysis of scalability, we found that fish adopt the same interaction rule in the pursuit behavior as when in large groups (Fig. 5). Overall, our work suggests that reverse engineering the control law in schooling fish using virtual conspecifics offers a complementary approach to traditional methods in both biology and engineering. It is valuable not only for systematically exploring potential internal SMCs in biological systems but also for designing controllers that are efficient and robust, requiring minimal sensing and computational resources.

MATERIALS AND METHODS

Methodological overview

We developed and used a VR platform to reverse engineer the SMC algorithm for schooling behavior (fig. S1). To confirm its effectiveness, we compared the speed control of an RF to another RF in a traditional platform with that to a VF in our system. Subsequently, we conducted open-loop experiments in the virtual environment with a single VF, where we controlled the leader's swimming properties, such as average speed, patterns, and visibility. By doing so, we developed a biologically inspired proportional-derivative control model for the following behavior and verified its assumptions. Furthermore, we estimated the model through various methods, including simulations, experiments in the VR system, experiments with two virtual leaders, and tests with three types of robots (terrestrial, airborne, and watercraft).

The VR platform

The test arena was bowl shaped, holding 4.5 liters of water, with a depth in the center of 9.1 cm and a diameter of 33.8 cm. The bowl was made from a material that is opaque to visible light but transparent to infrared light, allowing us to illuminate it from below with infrared light (wavelength of 850 nm) for tracking purposes. Positioned above the bowl were four Basler acA640 cameras, capturing images at 100 frames per second in real time. The three-dimensional (3D) position of the RF was reconstructed from its detected position in each view using blob detection. With these reconstructed 3D positions, we tracked the fish's movements on the basis of an extended Kalman filter and the nearest neighbor standard filter for data association. An LED (light-emitting diode) DLP (digital light processing) projector (Optoma ML500) illuminated the entire surface of the bowl to allow us to present the virtual scene in the visible light spectrum. To ensure accurate projection, the projected image was mapped onto the 3D curvature of the bowl using a calibration model of the display geometry. A grid was rendered during calibration, mapping each pixel to its corresponding geometric coordinates. The anamorphic illusion was applied to render the image as a 3D scene from the correct perspective of the RF. A VF, modeled in Blender (Blender Foundation) on the basis of juvenile zebrafish [26 days postfertilization (dpf), 1 cm], was rendered within the system to interact with freely swimming RF (24 to 27 dpf, 1 ± 0.1 cm) in 3D (*20*, *50*). In the Matrix setup, similar to (*28*), the RF's position and orientation were tracked on one machine and transferred in real time to another machine via a socket connection, allowing for seamless bidirectional communication between the two systems. For further details, please refer to our previous work (*20*, *50*).

VR experiments

We conducted experiments with zebrafish (*D. rerio*) of age 24 to 26 dpf raised in a room at 28°C on a 16-hour light, 8-hour dark cycle. The variation in age was to allow us to always use fish of a similar body length (1 ± 0.1 cm). Four hundred and ninety-eight zebrafish were used (see table S1). Experiments were conducted in a fish VR setup procured from Loopbio GmbH [refer to ref. (*20*) for details]. After a fish was introduced into the arena (a bowl-shaped container with a diameter of 34 cm and a depth of 9 cm at the water level),

we allowed the fish to acclimate to the environment for 20 min. This was followed by a 10-min control, during which the fish was presented with a single virtual conspecific (1 cm in body length) swimming in a circle with a diameter of 16 cm. After this, the RF was exposed to the VF, initialized with various swimming conditions (Supplementary Methods). Each experiment lasted 90 min. We analyzed the data using a custom Python 3.7 code. All experiments were conducted in accordance with the animal ethics permit approved by Regierungspräsidium Freiburg, G-16/116, G-17/88, and G-17/170.

Simulations

We used the BioPD algorithm to simulate the behavior of following a virtual leader in the VR experiment, as well as a real leader in a pair of fish performing leader-follower behavior extracted from RF data. For following the virtual leader, we set the follower's initial position to a range of −0.05 to 0.05 m on the x axis and −0.05 to 0 m on the y axis. We introduced variability by adding white noise to the follower's speed control, with a standard variance of 0.016 for the x axis and 0.45 times the average speed of the follower for the y axis. The maximum swimming speed was limited to 0.1 m/s. In contrast, for following an RF leader, we initialized the geometry position and swimming probabilities of the follower to match the starting point of leader-follower behavior in the pair of RF swimming in the same arena. The only difference in this model from the previous one is that the leader is extracted from RF leader data, which dynamically changes both average swimming speeds and directions. No noise was added in the second simulation.

Parameter estimation for the model

The BioPD model has four primary parameters (r_x, r_y, K_p, and K_d), which we determined by measuring RF data collected in the VR experiments. In the following behavior, when the distance between the leader and the follower was larger than the threshold distance r_x (r_y), the follower reduced its speed to follow the leader. Therefore, we modeled the turning point of speed as a first-order Gaussian derivative function, with the threshold distance corresponding to the peak of the function. We determined the threshold distance by bootstrapping (Supplementary Methods). Given that the follower must be within the distance threshold to catch up with the leader, we simplified the model to a traditional PD controller. By analyzing the PD controller, we found that the average swimming speed of the leader and follower is determined by a first-order linear function, where the slope is determined by K_d only and the intercept is determined by both K_p and K_d. We obtained these two parameters through a similar bootstrap analysis, and detailed derivations are given in Supplementary Methods.

Robotic experiments

We tested both BioPD and an optimal controller on four different types of robots: the Crazyflie drone (*42*), the SunFounder Robot PiCar-X, the Osoyoo Robot Pi Car, and a robot boat. To create a virtual leader for the robots to follow, we programmed it to move in a sinusoidal curve. We applied BioPD with the same mathematical model and parameters, which were scaled by the body size of the robots. In addition, we considered an MPC based on our previous study (*41*). To achieve the best performance with MPC, parameters were optimized for each type of robot. Further details can be found in Supplementary Methods.

Statistical analysis

We applied bootstrap resampling to estimate the variability in the relationships between lateral speed (v_x) and position in x, as well as forward speed (v_y) and position in y. Specifically, we resampled the collected data 100 times and plotted the average trends along with their variability, as shown in Fig. 2 (G and H). To evaluate the similarity between RF interactions in the physical world and those in the Matrix, we computed the root mean square deviation of lateral speed (v_x) and forward speed (v_y) as functions of the neighbor's position. Data from 22 real interaction pairs in the physical world were pooled to serve as a reference. We then compared this reference with the root mean square deviation of the remaining 24 real pairs and 24 virtual (the Matrix) pairs. Kolmogorov-Smirnov tests revealed no significant differences between the real and virtual conditions (lateral speed: $P = 0.26$; forward speed: $P = 0.9$). To further check the similarity among the simulations, the BioPD model, and the Turing test, we applied the Jensen-Shannon divergence (JSD). The results showed minimal divergence: JSD = 0.03 for forward swimming between simulations and the model (Fig. 4E), JSD = 0.0 for turning speed between simulations and the model (Fig. 4F), JSD = 0.08 for forward swimming between RF and the model in the Turing test (Fig. 4G), and JSD = 0.0 for turning speed between RF and the model in the Turing test (Fig. 4H). A standard box plot—featuring the median, interquartile range, and potential outliers—was used to illustrate the deviation between the robots' trajectories and the desired path, as shown in Fig. 5 (H to K).

Supplementary Materials

This PDF file includes:

Supplementary Methods
Figs. S1 to S29
Table S1

REFERENCES AND NOTES

1. S. Camazine, J.-L. Deneubourg, N. R. Frank, J. Sneyd, G. Theraulaz, E. Bonabeau, *Self-Organization in Biological Systems* (Princeton Univ. Press, 2003).
2. D. J. T. Sumpter, *Collective Animal Behavior* (Princeton Univ. Press, 2010).
3. T. S. Deisboeck, I. D. Couzin, Collective behavior in cancer cell populations. *Bioessays* **31**, 190–197 (2009).
4. J. Buhl, D. J. T. Sumpter, I. D. Couzin, J. J. Hale, E. Despland, E. R. Miller, S. J. Simpson, From disorder to order in marching locusts. *Science* **312**, 1402–1406 (2006).
5. P. Ramdya, P. Lichocki, S. Cruchet, L. Frisch, W. Tse, D. Floreano, R. Benton, Mechanosensory interactions drive collective behaviour in *Drosophila*. *Nature* **519**, 233–236 (2015).
6. A. J. W. Ward, J. E. Herbert-Read, D. J. T. Sumpter, J. Krause, Fast and accurate decisions through collective vigilance in fish shoals. *Proc. Natl. Acad. Sci. U.S.A.* **108**, 2312–2315 (2011).
7. A. Berdahl, C. J. Torney, C. C. Ioannou, J. J. Faria, I. D. Couzin, Emergent sensing of complex environments by mobile animal groups. *Science* **339**, 574–576 (2013).
8. R. C. Hinz, G. G. de Polavieja, Ontogeny of collective behavior reveals a simple attraction rule. *Proc. Natl. Acad. Sci. U.S.A.* **114**, 2295–2300 (2017).
9. M. Ballerini, N. Cabibbo, R. Candelier, A. Cavagna, E. Cisbani, I. Giardina, V. Lecomte, A. Orlandi, G. Parisi, A. Procaccini, M. Viale, V. Zdravkovic, Interaction ruling animal collective behavior depends on topological rather than metric distance: Evidence from a field study. *Proc. Natl. Acad. Sci. U.S.A.* **105**, 1232–1237 (2008).
10. A. Flack, M. Nagy, W. Fiedler, I. D. Couzin, M. Wikelski, From local collective behavior to global migratory patterns in white storks. *Science* **360**, 911–914 (2018).
11. M. Moussaid, D. Helbing, G. Theraulaz, How simple rules determine pedestrian behavior and crowd disasters. *Proc. Natl. Acad. Sci. U.S.A.* **108**, 6884–6888 (2011).
12. A. C. Gallup, J. J. Hale, D. J. T. Sumpter, S. Garnier, A. Kacelnik, J. R. Krebs, I. D. Couzin, Visual attention and the acquisition of information in human crowds. *Proc. Natl. Acad. Sci. U.S.A.* **109**, 7245–7250 (2012).
13. G.-Z. Yang, J. Bellingham, P. E. Dupont, P. Fischer, L. Floridi, R. Full, N. Jacobstein, V. Kumar, M. McNutt, R. Merrifield, B. J. Nelson, B. Scassellati, M. Taddeo, R. Taylor, M. Veloso,

Z. L. Wang, R. Wood, The grand challenges of *Science Robotics*. *Sci. Robot.* **3**, eaar7650 (2018).
14. J. Werfel, K. Petersen, R. Nagpal, Designing collective behavior in a termite-inspired robot construction team. *Science* **343**, 754–758 (2014).
15. F. Berlinger, M. Gauci, R. Nagpal, Implicit coordination for 3D underwater collective behaviors in a fish-inspired robot swarm. *Sci. Robot.* **6**, eabd8668 (2021).
16. M. Nagy, Z. Akos, D. Biro, T. Vicsek, Hierarchical group dynamics in pigeon flocks. *Nature* **464**, 890–893 (2010).
17. S. Marras, R. S. Batty, P. Domenici, Information transfer and antipredator maneuvers in schooling herring. *Adapt. Behav.* **20**, 44–56 (2012).
18. K. R. Pilkiewicz, B. H. Lemasson, M. A. Rowland, A. Hein, J. Sun, A. Berdahl, M. L. Mayo, J. Moehlis, M. Porfiri, E. Fernández-Juricic, S. Garnier, E. M. Bollt, J. M. Carlson, M. R. Tarampi, K. L. Macuga, L. Rossi, C. C. Shen, Decoding collective communications using information theory tools. *J. R. Soc. Interface* **17**, 20190563 (2020).
19. A. Laan, R. G. de Sagredo, G. G. de Polavieja, Signatures of optimal control in pairs of schooling zebrafish. *Proc. R. Soc. B* **284**, 20170224 (2017).
20. J. R. Stowers, M. Hofbauer, R. Bastien, J. Griessner, P. Higgins, S. Farooqui, R. M. Fischer, K. Nowikovsky, W. Haubensak, I. D. Couzin, K. Tessmar-Raible, A. D. Straw, Virtual reality for freely moving animals. *Nat. Methods* **14**, 995–1002 (2017).
21. H. Naik, R. Bastien, N. Navab, I. D. Couzin, Animals in virtual environments. *IEEE Trans. Vis. Comput. Graph.* **26**, 2073–2083 (2020).
22. S. Sayin, E. Couzin-Fuchs, I. Petelski, Y. Günzel, M. Salahshour, C.-Y. Lee, J. M. Graving, L. Li, O. Deussen, G. A. Sword, I. D. Couzin, The behavioral mechanisms governing collective motion in swarming locusts. *Science* **387**, 995–1000 (2025).
23. G. Dumas, G. C. de Guzman, E. Tognoli, J. A. S. Kelso, The human dynamic clamp as a paradigm for social interaction. *Proc. Natl. Acad. Sci. U.S.A.* **111**, E3726–E3734 (2014).
24. A. A. Sharp, M. B. Oneil, L. F. Abbott, E. Marder, The dynamic clamp: Artificial conductances in biological neurons. *Trends Neurosci.* **16**, 389–394 (1993).
25. M. J. McHenry, G. V. Lauder, The mechanical scaling of coasting in zebrafish (*Danio rerio*). *J. Exp. Biol.* **208**, 2289–2301 (2005).
26. A. Strandburg-Peshkin, D. Papageorgiou, M. C. Crofoot, D. R. Farine, Inferring influence and leadership in moving animal groups. *Philos. Trans. R. Soc. B* **373**, 20170006 (2018).
27. M. Mischiati, H. T. Lin, P. Herold, E. Imler, R. Olberg, A. Leonardo, Internal models direct dragonfly interception steering. *Nature* **517**, 333–338 (2015).
28. M. Karakaya, S. Macrì, M. Porfiri, Behavioral teleporting of individual ethograms onto inanimate robots: Experiments on social interactions in live zebrafish. *iScience* **23**, 101418 (2020).
29. L. Ristroph, A. J. Bergou, G. Ristroph, K. Coumes, G. J. Berman, J. Guckenheimer, Z. J. Wang, I. Cohen, Discovering the flight autostabilizer of fruit flies by inducing aerial stumbles. *Proc. Natl. Acad. Sci. U.S.A.* **107**, 4820–4824 (2010).
30. M. J. McHenry, J. L. Johansen, A. P. Soto, B. A. Free, D. A. Paley, J. C. Liao, The pursuit strategy of predatory bluefish (*Pomatomus saltatrix*). *Proc. R. Soc. B Biol. Sci.* **286**, 20182934 (2019).
31. A. M. Hein, D. L. Altshuler, D. E. Cade, J. C. Liao, B. T. Martin, G. K. Taylor, An algorithmic approach to natural behavior. *Curr. Biol.* **30**, R663–R675 (2020).
32. M. S. Madhav, N. J. Cowan, The synergy between neuroscience and control theory: The nervous system as inspiration for hard control challenges. *Annu. Rev. Control Robot. Auton. Syst.* **3**, 243–267 (2020).
33. S. C. Whitehead, S. Leone, T. Lindsay, M. R. Meiselman, N. J. Cowan, M. H. Dickinson, N. Yapici, D. L. Stern, T. Shirangi, I. Cohen, Neuromuscular embodiment of feedback control elements in *Drosophila* flight. *Sci. Adv.* **8**, eabo7461 (2022).
34. P. Ramdya, A. J. Ijspeert, The neuromechanics of animal locomotion: From biology to robotics and back. *Sci. Robot.* **8**, eadg0279 (2023).
35. T. J. Prescott, S. P. Wilson, Understanding brain functional architecture through robotics. *Sci. Robot.* **8**, eadg6014 (2023).
36. J. Larsch, H. Baier, Biological motion as an innate perceptual mechanism driving social affiliation. *Curr. Biol.* **28**, 3523–3532.e4 (2018).
37. T. Pasternak, M. W. Greenlee, Working memory in primate sensory systems. *Nat. Rev. Neurosci.* **6**, 97–107 (2005).
38. V. H. Sridhar, L. Li, D. Gorbonos, M. Nagy, B. R. Schell, T. Sorochkin, N. S. Gov, I. D. Couzin, The geometry of decision-making in individuals and collectives. *Proc. Natl. Acad. Sci. U.S.A.* **118**, e2102157118 (2021).
39. T. Walter, I. D. Couzin, TRex, a fast multi-animal tracking system with markerless identification, and 2D estimation of posture and visual fields. *eLife* **10**, e64000 (2021).
40. J. D. Davidson, M. M. G. Sosna, C. R. Twomey, V. H. Sridhar, S. P. Leblanc, I. D. Couzin, Collective detection based on visual information in animal groups. *J. R. Soc. Interface* **18**, 20210142 (2021).
41. W. Wang, L. A. Mateos, S. Park, P. Leoni, B. Gheneti, F. Duarte, C. Ratti, D. Rus, "Design, modeling, and nonlinear model predictive tracking control of a novel autonomous surface vehicle," in *Proceedings of the 2018 IEEE International Conference on Robotics and Automation (ICRA)* (IEEE, 2018), pp. 6189–6196.
42. W. Giernacki, M. Skwierczynski, W. Witwicki, P. Wronski, P. Kozierski, "Crazyflie 2.0 quadrotor as a platform for research and education in robotics and control engineering," in *Proceedings of the 22nd International Conference on Methods and Models in Automation and Robotics (MMAR)* (IEEE, 2017), pp. 37–42.
43. K. Ogata, *Modern Control Engineering* (Prentice Hall, 2010).
44. D. Gorbonos, N. S. Gov, I. D. Couzin, Geometrical structure of bifurcations during spatial decision-making. *PRX Life* **2**, 013008 (2024).
45. J. Thomas, J. Welde, G. Loianno, K. Daniilidis, V. Kumar, Autonomous flight for detection, localization, and tracking of moving targets with a small quadrotor. *IEEE Robot. Autom. Lett.* **2**, 1762–1769 (2017).
46. D. Panagou, V. Kumar, Cooperative visibility maintenance for leader–follower formations in obstacle environments. *IEEE Trans. Robot.* **30**, 831–844 (2014).
47. J.-M. Mongeau, S. N. Sponberg, J. P. Miller, R. J. Full, Sensory processing within cockroach antenna enables rapid implementation of feedback control for high-speed running maneuvers. *J. Exp. Biol.* **218**, 2344–2354 (2015).
48. D. Natesan, N. Saxena, Ö. Ekeberg, S. P. Sane, Tuneable reflexes control antennal positioning in flying hawkmoths. *Nat. Commun.* **10**, 5593 (2019).
49. C. H. Brighton, A. L. R. Thomas, G. K. Taylor, Terminal attack trajectories of peregrine falcons are described by the proportional navigation guidance law of missiles. *Proc. Natl. Acad. Sci. U.S.A.* **114**, 13495–13500 (2017).
50. G. Amichay, L. Li, M. Nagy, I. D. Couzin, Revealing the mechanism and function underlying pairwise temporal coupling in collective motion. *Nat. Commun.* **15**, 4356 (2024).

Acknowledgments: We thank all members of the Department of Collective Behavior who assisted with the project: R. Bastien for discussions at the beginning of the project, S. Zhao for fruitful discussions regarding the feedback control, J. Davidson for data analysis suggestions, A. Gonzalez-Garcia for helping conduct experiments on watercraft, and N. Troje for insightful comments. We thank A. Poehlmann, J. Stowers, and M. Hofbauer from Loopbio GmbH for technical support with the VR systems and the animal care staff at the University of Konstanz, including A. Bruttel, C. Bauer, J. Weglarski, and D. Leo, for help in taking care of and preparing fish for experiments. We thank M. Günther, J. Peters, S. Wang, G. Wang, K. Kumari, and I. Hachen for help in running robot experiments. **Funding:** This work was supported by the following: Deutsche Forschungsgemeinschaft (DFG, German Research Foundation) under Germany's Excellence Strategy–EXC 2117-422037984; to I.D.C.: the Max Planck Society, the European Union's Horizon 2020 Research and Innovation Programme under Marie Skłodowska-Curie Grant 860949, the DFG Gottfried Wilhelm Leibniz Prize 2022 584/22, the Struktur-und Innovationsfonds für die Forschung of the State of Baden-Württemberg, the PathFinder European Innovation Council Work Programme 101098722, and the Office of Naval Research grant N0001419-1-2556; to M.N.: Hungarian Academy of Sciences Grant 95152 (to the MTA-ELTE "Lendület" Collective Behaviour Research Group) and Eötvös Loránd University; to L.L.: Messer Foundation Award and Sino-German grant M-0541; to W.W. and D.R.: a grant from the Amsterdam Institute for Advanced Metropolitan Solutions (AMS) in the Netherlands; to W.W.: a startup grant provided by the Department of Mechanical Engineering and the College of Engineering at the University of Wisconsin-Madison, and the Office of the Vice Chancellor for Research and Graduate Education with funding from the Wisconsin Alumni Research Foundation. **Author contributions:** L.L., M.N., and I.D.C. conceived the idea and designed the project. L.L. conducted the fish VR experiments and collected data. L.L. and G.A. conducted experiments and collected the 3D tracking and matrix data. L.L. and M.N. analyzed data with contributions from I.D.C. and O.D. L.L., R.W., and W.W. conducted experiments on robots and collected data with contributions from O.D. and D.R. L.L., M.N., and I.D.C. wrote the initial draft, and all authors contributed to the revision of the text. **Competing interests:** The authors declare that they have no competing interests. **Data and materials availability:** All data needed to support the conclusions of this manuscript are included in the main text or Supplementary Materials. Source data and code are available via Dryad (DOI: 10.5061/dryad.np5hqc02k).

Submitted 26 May 2024
Accepted 2 April 2025
Published 30 April 2025
10.1126/scirobotics.adq6784

Science Robotics

Reverse engineering the control law for schooling in zebrafish using virtual reality

Liang Li, Máté Nagy, Guy Amichay, Ruiheng Wu, Wei Wang, Oliver Deussen, Daniela Rus, and Iain D. Couzin

Sci. Robot. **10** (101), eadq6784. DOI: 10.1126/scirobotics.adq6784

Science Robotics (ISSN 2470-9476) is published by the American Association for the Advancement of Science. 1200 New York Avenue NW, Washington, DC 20005. The title *Science Robotics* is a registered trademark of AAAS.